Transient Ru-methyl formate intermediates generated with bifunctional transfer hydrogenation catalysts

Richard H. Perry, Kristen R. Brownell, Konstantin Chingin, Thomas J. Cahill III, Robert M. Waymouth, and Richard N. Zare[1]

Department of Chemistry, Stanford University, Stanford, CA 94305-5080

Contributed by Richard N. Zare, November 17, 2011 (sent for review October 10, 2011)

Desorption electrospray ionization (DESI) coupled to high-resolution Orbitrap mass spectrometry (MS) was used to study the reactivity of a (β-amino alcohol)(arene)RuCl transfer hydrogenation catalytic precursor in methanol (CH_3OH). By placing [(*p*-cymene)$RuCl_2$]$_2$ on a surface and spraying a solution of β-amino alcohol in methanol, two unique transient intermediates having lifetimes in the submillisecond to millisecond range were detected. These intermediates were identified as Ru (II) and Ru (IV) complexes incorporating methyl formate ($HCOOCH_3$). The Ru (IV) intermediate is not observed when the DESI spray solution is sparged with Ar gas, indicating that O_2 dissolved in the solvent is necessary for oxidizing Ru (II) to Ru (IV). These proposed intermediates are supported by high-resolution and high mass accuracy measurements and by comparing experimental to calculated isotope profiles. Additionally, analyzing the bulk reaction mixture using gas chromatography-MS and nuclear magnetic resonance spectroscopy confirms the formation of $HCOOCH_3$. These results represent an example that species generated from the (β-amino alcohol)(arene)RuCl (II) catalytic precursor can selectively oxidize CH_3OH to $HCOOCH_3$. This observation leads us to propose a pathway that can compete with the hydrogen transfer catalytic cycle. Although bifunctional hydrogen transfer with Ru catalysts has been well-studied, the ability of DESI to intercept intermediates formed in the first few milliseconds of a chemical reaction allowed identification of previously unrecognized intermediates and reaction pathways in this catalytic system.

organometallic catalysis | reaction intermediates | ruthenium | kinetics

Catalytic transfer hydrogenation (CTH) is an efficient method for the enantioselective reduction of multiple bonds (e.g., C═O and C═NR) in chemical and pharmaceutical syntheses (1–4). Typically, a hydrogen donor such as isopropanol is used as a convenient reducing agent and is oxidized to its corresponding ketone (5). As a catalytic version of the classical Meerwein–Pondorf–Verley reduction/Oppenaur oxidation (6–10), CTH provides a mild method for both ketone reduction and alcohol oxidation. Previous studies show that methanol (CH_3OH) can serve as a hydrogen donor for (arene)Ru complexes ligated by β-amino alcohols (11), but the nature of the oxidized products from CH_3OH has not been previously characterized (12). Additionally, some Pd and Ru (13, 14) catalysts can oxidize CH_3OH to methyl formate ($HCOOCH_3$), but selective oxidation to methyl formate has not been observed previously for a transfer hydrogenation catalysis.

Fig. 1 shows the mechanism proposed by Kenney, Heck, Walgrove, and Wills (15) for CTH when Fig. 1, **1** is treated with β-amino alcohol ligands in the presence of a base. Ligation of the cymene dimer Fig. 1, **1** with ligand Fig. 1, **2** generates the Ru-Cl catalyst precursor Fig. 1, **3**, which undergoes dehydrohalogenation to form the Ru-amide Fig. 1, **4**. An outer-sphere concerted hydrogen transfer of α-C—H to Ru and —O—H to the nitrogen atom of the ligand affords the Ru-H Fig. 1, **5**. The interconversion of Ru-amide Fig. 1, **4** and Ru-H Fig. 1, **5** by a bifunctional transfer of a hydride and a proton effects the oxidation of alcohols and reduction of ketones (5, 11, 15–20).

Electrospray ionization-mass spectrometry (ESI-MS) is well established for studying reaction mechanisms in solution (21–23). A previous ESI-MS study of CTH (Fig. 1) detected the Ru-Cl Fig. 1, **3**, Ru-amide Fig. 1, **4**, and Ru-H Fig. 1, **5** of CTH in bulk reaction mixtures (reaction time of a few minutes) (15). Ambient ionization methods (24–26) such as desorption electrospray ionization (DESI) (27–29) provide a simpler approach to intercepting reactive species without prior sample preparation (30–35). We recently demonstrated that DESI can intercept CTH intermediates in solution on the millisecond time scale (36). However, the low resolution and low mass accuracy of the quadrupole ion trap mass spectrometer used previously (36) prevented unambiguous identification of the ionic species.

Although Ru complexes have been well-investigated for CTH, herein we provide evidence for unique reaction intermediates derived from methyl formate that were not observed in earlier mechanistic studies when methanol is used as the hydrogen donor. These intermediates were intercepted on the millisecond time scale using DESI (36) and then detected with a high-resolution Orbitrap (37–39) mass spectrometer. The observation of these intermediates indicates that reactive species generated from activation of (β-amino alcohol) (arene)Ru (II) complexes can selectively oxidize CH_3OH to $HCOOCH_3$ (40–43). Additionally, when trace oxygen (O_2) is present in the CH_3OH, we find that Ru (II) is converted to a Ru (IV) hydroxo species complexed to $HCOOCH_3$*. These observations attest to both the high reactivity of (β-amino alcohol)(arene)Ru (II) complexes as well as their sensitivity and reactivity toward adventitious O_2.

Results and Discussion

To characterize the intermediates and products formed upon reaction of CH_3OH with complexes derived from the Ru-Cl Fig. 1, **3**, a DESI experiment was carried out as previously described (36). An aliquot (5 μL) of [$RuCl_2$(*p*-cymene)]$_2$ (Fig. 1, **1**; 10^{-2} M in CH_2Cl_2) was deposited on paper affixed to a glass slide and a CH_3OH solution containing (1***R***, 2***S***)-*cis*-1-amino-2-indanol (Fig. 1, **2**; 10^{-4} M) was sprayed onto the surface by a DESI source (*SI Appendix*, Fig. S1; 5 kV or 0 kV spray voltage; unless specified otherwise; all data presented is for 5 kV). The solution containing Fig. 1, **2** was continuously supplied to the DESI source at a rate of 20 μL/min using a syringe pump and the spray was produced by sheath gas (N_2) flowing at a rate of 0.6 L/min. The reaction is initiated when the spray containing Fig. 1, **2** impacts Fig. 1, **1** on the surface. The reactive species are generated in the liquid-phase environment of the secondary microdroplets (approximately 2 μm in diameter) (44) as they travel to the inlet

Author contributions: R.H.P., K.R.B., R.M.W., and R.N.Z. designed research; R.H.P., K.R.B., K.C., and T.J.C. performed research; R.H.P., K.R.B., T.J.C., and R.M.W. analyzed data; R.H.P., R.M.W., and R.N.Z. wrote the paper.

The authors declare no conflict of interest.

See Commentary on page 2186.

*An alternate, isobaric formulation is *SI Appendix*, Fig. S15, **7a**, the adduct of $HOCOOCH_3$ and the cationic Ru (II) fragment derived from Fig. 1, **4**.

[1]To whom correspondence should be addressed. E-mail: zare@stanford.edu.

This article contains supporting information online at www.pnas.org/lookup/suppl/doi:10.1073/pnas.1118934109/-/DCSupplemental.

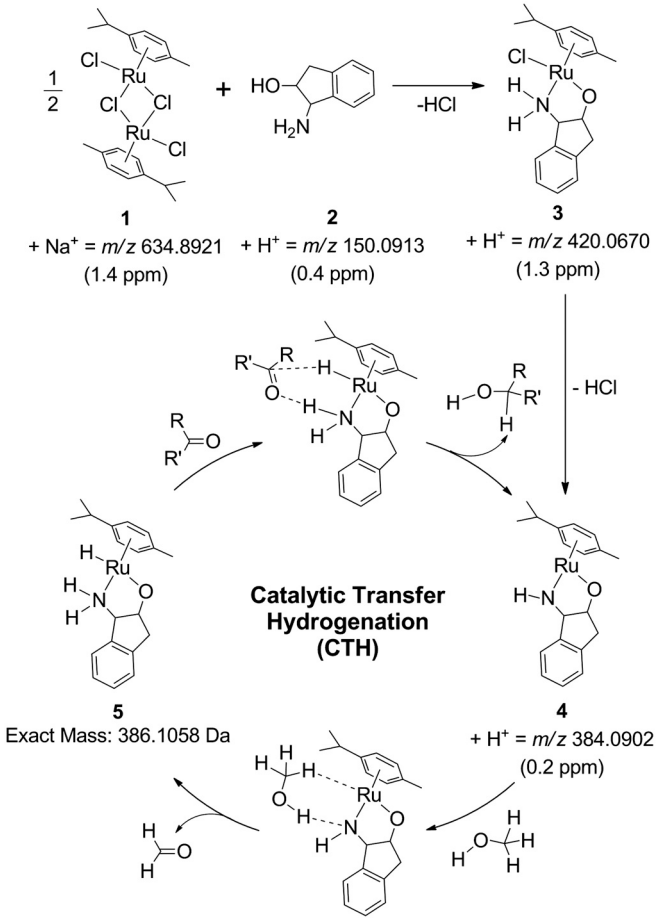

Fig. 1. Proposed mechanism (15) for catalytic transfer hydrogenation using $[RuCl_2(p\text{-cymene})]_2$ treated with (1***R***, 2***S***)-*cis*-1-amino-2-indanol. Ions detected in Orbitrap mass spectra are indicated below the chemical structures along with corresponding m/z values and mass accuracy measurements in parts-per-million (ppm). The mass accuracy is calculated using the relationship ppm = [|experimentalm/z-theoreticalm/z|/theoreticalm/z × 10^6]. The Ru hydride catalyst **5** (exact mass = 386.1058 Da) was not observed in acquired DESI mass spectra. Transition states for the concerted hydrogen transfers have been indicated in this figure but not labeled.

of a mass spectrometer (*SI Appendix*, Fig. S1). The speed of the secondary microdroplets (approximately 4 m/s) (44) and the short distance from the impact site to the mass spectrometer inlet (0.5 cm) results in a reaction time of a few milliseconds before reaction is quenched by the formation of gas-phase ions (36).

The resulting DESI mass spectrum (Fig. 2*A*) shows ions in the m/z range 500–650 corresponding to [Ru]—OCH_3 and [Ru]—OH species (*SI Appendix*, Fig. S2; square brackets represent other coordinations and bonds to the metal) formed from reaction of Fig. 1, **1** with CH_3OH and adventitious H_2O with loss of HCl. The assignments of these reaction intermediates are supported by experiments using CD_3OD and D_2O showing mass shifts corresponding to the number of —OH and —OCH_3 groups bonded to Ru (*SI Appendix*, Figs. S3 and S4). The predominant ion at m/z = 576.9360 corresponds to $[\mathbf{1} - Cl]^+$ ($C_{20}H_{28}Cl_3Ru_2$; 1.1 ppm) and the intact sodiated Ru complex, $[\mathbf{1} + Na]^+$, is observed at m/z 634.8921 ($C_{20}H_{28}Cl_4NaRu_2$; 1.4 ppm). In addition, intermediates formed in the first few milliseconds of the reaction that generates Ru-Cl Fig. 1, **3** are detected (see *SI Appendix*, Fig. S5 for proposed structures). These species include the initial association of Fig. 1, **1** with Fig. 1, **2** ($[\mathbf{1} + \mathbf{2} + H]^+$; m/z 763.9937; 0.2 ppm) followed by subsequent losses of HCl ($[\mathbf{1} + \mathbf{2} - Cl]^+$, m/z 726.0178, 0.7 ppm; $[\mathbf{1} + \mathbf{2} - 2Cl - H]^+$, m/z 690.0424, 0.4 ppm), which agrees with proposed associative mechanisms (5). From this point forward,

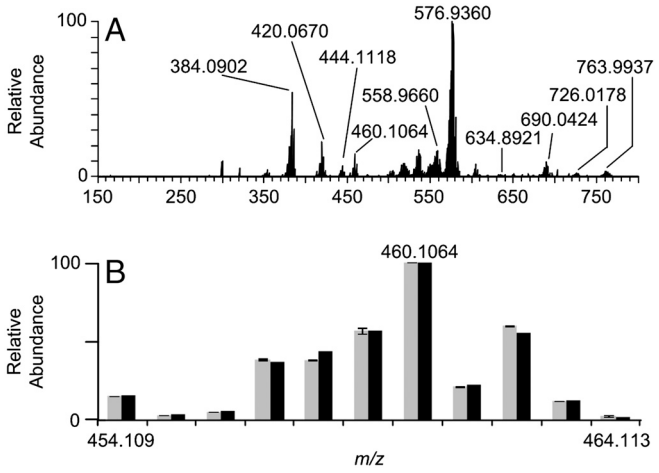

Fig. 2. (*A*) DESI Orbitrap mass spectrum (background subtracted) showing some of the intermediates formed in the reaction of Fig. 1, **1** with Fig. 1, **2** (see *SI Appendix*, Fig. S6 for m/z 800–m/z 1,500). Resolution = approximately 80,000 at m/z 400 and mass accuracy is less than 3 ppm using $[\mathbf{2} + H]^+$ at m/z 150.0913 as a calibration mass. (*B*) Isotope profile for Fig. 4, **7** comparing experimental (gray) and calculated (black) distributions [‡].

specific species will be referred to using the m/z value of the most intense peak of the isotope distribution. Although these intermediates are predicted, their high reactivity and short lifetimes prevented isolation and detection (5, 11, 15) prior to this study.

Ions that are generated include complex Fig. 1, **3** at m/z 420.0670 $[C_{19}H_{24}ONRuCl]^+$ and Fig. 1, **4** at m/z 384.0902 $[C_{19}H_{23}ONRu]^+$ (Figs. 1 and 2*A*), which agree with previous ESI-MS (15) and DESI-MS (36) results. The [Ru]—H Fig. 1, **5** was observed by NMR (Fig. 3) (45, 46) but not by DESI-MS (Fig. 2*A*). In addition to Fig. 1, **3** and **4**, the high mass accuracy and resolving power of the Orbitrap allowed identification of two transient species at m/z 444.1118 (Fig. 4, **6**) and m/z 460.1064 (Fig. 4, **7**) (Figs. 2 and 4).

When potassium hydroxide (KOH; 10^{-4} M in CH_3OH) is added to the reagent spray the same reactive species are observed (but with different relative intensities; *SI Appendix*, Fig. S7) along with corresponding potassium adducts such as $[\mathbf{1} + K]^+$ at m/z 650.8669 ($C_{20}H_{28}Cl_4KRu_2$; 3.3 ppm). KOH is typically added to solutions of Fig. 1, **1** and **2** to facilitate dehydrohalogenation (5). In DESI experiments that do not have KOH in the reagent spray (Fig. 2), it is likely that adventitious H_2O displaces the Cl ligands of Fig. 1, **1** and **3**, thereby activating the catalyst precursor. (47). In addition, when no spray voltage is applied (i.e., 0 kV) the same transient species are observed but the sensitivity is approximately three times lower (36), which indicates that these species are generated without applying any potential to the solution.

The first step toward identifying the structures of the intermediates at m/z 444.1118 and m/z 460.1064 is to determine their elemental compositions from high-resolution Orbitrap mass spectra (Fig. 2). The observation that the species at m/z 460.1064 contains Fig. 1, **2** (36), coupled with the known reagent structures and compositions (Fig. 1), high mass accuracy and high resolution of Orbitrap mass spectra, and isotope profiles showing that the species at m/z 460.1064 is singly charged (viz. the charge comes from Ru^+, Na^+, or H^+) with only one Ru atom (Fig. 2*B*), which indicates that there are only 17 possible elemental compositions. The calculation parameters are shown in *SI Appendix*, Table S1, and the possible elemental formulas are listed in *SI Appendix*, Table S2.

[‡]Isotope ratios are calculated by using Qual Browser software from Thermo Fisher Scientific and only peaks with signal-to-noise ratio greater than three were considered. Each error bar represents one standard deviation calculated from three measurements, with 10 spectra averaged per measurement.

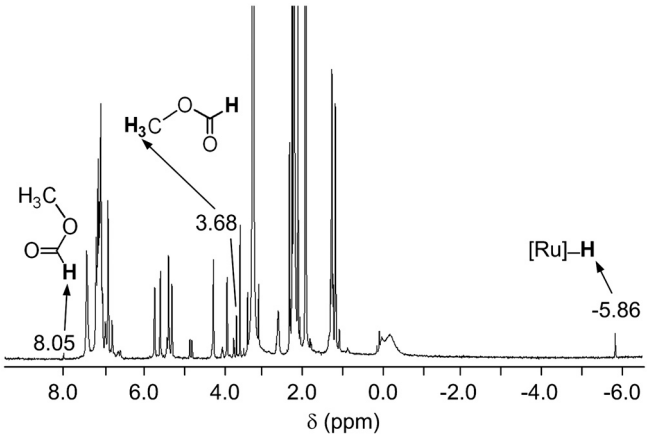

Fig. 3. ^{1}H NMR spectrum of a reaction mixture containing 0.024 mmol Fig. 1, **3**, 5 eq. KOH, and 10 eq. CH_3OH in CD_3CN (reaction time is 1 h). The chemical shifts for $HCOOCH_3$ and the monohydride catalyst ([Ru]-H) are labeled.

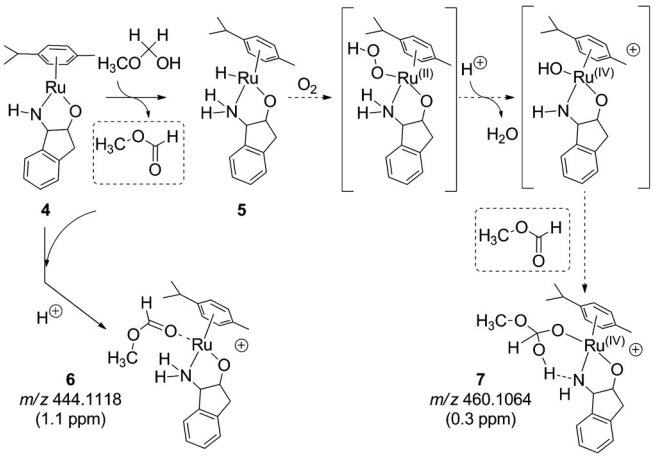

Fig. 4. Proposed mechanism for the formation of Ru-methyl formate intermediates (**6** and **7**) in transfer hydrogenations catalyzed by Ru catalysts ligated with β-amino alcohols.

Of the possible elemental compositions for the ion at m/z 460.1064 (see *SI Appendix* for a description of the calculations), this species is assigned the elemental composition of $[C_{21}H_{28}O_4NRu]^+$ (formula 17 in *SI Appendix*, Table S2; exact mass of 460.1062 Da, which is 0.3 ppm from the experimental value). The calculated isotopic abundances for $[C_{21}H_{28}O_4NRu]^+$ have an average deviation of $2 \pm 1\%$ from the experimental values (Fig. 2*B*)†, providing further support for this assignment. For all the identified species in this study, the average deviations are less than 5% and mass accuracy is better than 5 ppm. Performing similar analyses for the intermediate at m/z 444.1118 produces nine elemental compositions (*SI Appendix*, Table S3, formulas 18–26), of which only $[C_{21}H_{28}O_3NRu]^+$ is feasible. Complexes Fig. 1, **3** and **4** (12), as well as the species at m/z 460.1064 and m/z 444.1118, contain *p*-cymene and a [Ru]—O— ligand bond. After accounting for the ligand (C_9H_9NO) and *p*-cymene ($C_{10}H_{14}$) in $[C_{21}H_{28}O_4NRu]^+$ and $[C_{21}H_{28}O_3NRu]^+$, the remaining elemental composition ($C_2H_5O_3$ and $C_2H_5O_2$) represent other organic substituents bound to the (C_9H_9NO) (*p*-cymene)Ru base structure of m/z 460.1064 and m/z 444.1118.

For m/z 444.1118, the elemental composition of $[C_{21}H_{28}O_3NRu]^+$ is most reasonably formulated as compound Fig. 4, **6**, the coordination of $HCOOCH_3$ to a cationic Ru fragment formed by protonation of the amide Fig. 4, **4**. The amide Fig. 1, **4** is evident in the DESI spectrum of the *p*-cymene dimer Fig. 1, **1** and ligand Fig. 1, **2** with CH_3OH as the reagent spray solution (Fig. 2*A*); the observation of the Ru—$HCOOCH_3$ intermediate Fig. 4, **6** indicates that oxidation of CH_3OH is occurring on the millisecond time scale of the DESI experiment. For m/z 460.1064, the elemental composition of $[C_{21}H_{28}O_4NRu]^+$ is formulated as Fig. 4, **7**, a Ru (IV) hydroxo species complexed to $HCOOCH_3$.

We posited that adventitious oxygen might be responsible for the formation of species Fig. 4, **7**. To test this, we repeated the DESI experiment under conditions where the CH_3OH spray solution was previously degassed by bubbling Ar through the spray solution (10^{-4} M of Fig. 1, **2** in CH_3OH) for 5 min prior to reaction with Fig. 1, **1** by DESI. Under these conditions, the peak at m/z 460.1046 disappears whereas peaks for other reactive species remain relatively unchanged compared to when the solution is not degassed (Fig. 5). This result indicates that O_2 dissolved in the solvent is essential to form m/z 460.1064.

To complement the DESI experiments and obtain further information on the nature of the organic species that might be generated in the presence of CH_3OH under inert conditions, Fig. 1, **3** (0.024 mmol) was treated with 5 equivalents (eq.) of KOH and 10 eq. of dried CH_3OH and monitored by ^{1}H NMR in deuterated acetonitrile (CD_3CN). The resulting NMR spectra of the mixture after 1 h (Fig. 3) and 24 h (*SI Appendix*, Fig. S8) show chemical shifts at 8.05 ppm and 3.68 ppm, which correspond to the H—C═O and H_3—C—O protons of $HCOOCH_3$. This assignment was confirmed by gas chromatography-mass spectrometry of the reaction mixture showing a peak at m/z 60 (*SI Appendix*, Fig. S9), and by comparison of the chemical shifts to that of pure $HCOOCH_3$ in CD_3CN (*SI Appendix*, Fig. S10). Coupling of the signals at 8.05 ppm and 3.68 ppm in two-dimensional correlation NMR spectroscopy (COSY) indicate that these protons are within a few chemical bonds, providing additional support for the identification of $HCOOCH_3$ (*SI Appendix*, Fig. S11). In addition to $HCOOCH_3$, the resonance at −5.86 ppm (Fig. 3) confirms the formation of the metal hydride Fig. 1, **5** in solution. Catalytic dehydrogenation of CH_3OH by Ru (II) complexes to form $HCOOCH_3$ has been observed previously by Shinoda and coworkers (13, 14), but to our knowledge selective dehydrogenation of CH_3OH to $HCOOCH_3$ with species known to catalyze transfer hydrogenation has not been previously demonstrated. Although an ion signal for the Ru-H Fig. 1, **5** (exact mass is 386.1058 Da) was not observed in acquired DESI mass spectra, the observation that $HCOOCH_3$ and the Ru-H Fig. 1, **5** are generated in the NMR experiments would suggest that the dehydrogenation of

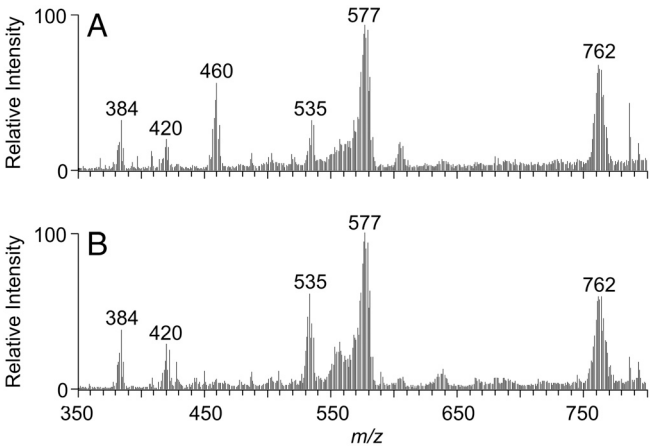

Fig. 5. (*A*) Mass spectrum of Fig. 1, **1** (5 μL of 10^{-2} M in CH_2Cl_2 deposited on paper) using a solution of Fig. 1, **2** (10^{-4} M in CH_3OH) in the DESI spray. (*B*) DESI mass spectrum after bubbling Ar through Fig. 1, **2** (10^{-4} M in CH_3OH) for 5 min.

†Average deviation = average value of |(calculated relative abundance) - (experimental relative abundance)| for each isotope.

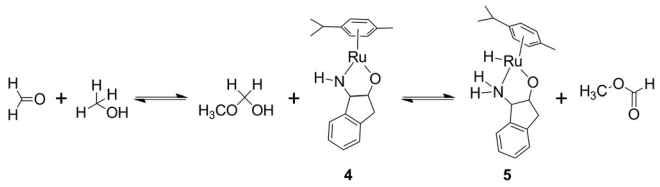

Fig. 6. Proposed mechanism for methanol oxidation to methyl formate during CTH.

methanol is mediated by the Ru-amide Fig. 1, **4**, as proposed for transfer hydrogenation.

A number of homogenous catalysts are known to oxidatively dehydrogenate CH_3OH to $HCOOCH_3$ (13, 14, 40–43) and formaldehyde (CH_2O) was proposed as a key intermediate (48–52). Although CH_3OH has been investigated previously as a hydrogen donor in CTH (12), the nature of the oxidized products from CH_3OH has not been previously characterized. Moreover, these previous observations when coupled with the structural information obtained from NMR provides important insights on the nature of the ions formed at m/z 444.1118 and m/z 460.1064 as observed by DESI.

Based on these discoveries we propose a mechanism similar to that of Pearson and Waymouth (40) involving initial oxidation of CH_3OH to form CH_2O, condensation of CH_2O and CH_3OH to produce a methyl hemiformal intermediate, and subsequent dehydrogenation of the hemiformal by Fig. 4, **4** to generate Fig. 4, **5** and $HCOOCH_3$ (Figs. 4 and 6). $HCOOCH_3$ can then coordinate with protonated amide Fig. 4, **4** to yield Fig. 4, **6**. In the presence of oxygen, competitive oxidation occurs. Although the mechanism by which this occurs is not yet clear, studies of aerobic oxidation with analogous Ir, Rh, and Ru transfer hydrogenation catalysts (53–56) allow some reasonable hypotheses to be made. One possibility is that oxidation of the Ru-H Fig. 4, **5** by dissolved O_2 generates a hydroperoxo–[Ru] intermediate (HOO—[Ru]). This intermediate could then undergo protonolysis with O—O bond heterolysis to yield a $[Ru^{(IV)}]$-OH species with loss of H_2O (57). The formation of high-valent metal-hydroxo complexes via metal-hydroperoxo intermediates from reaction with O_2 is a known pathway for various transition metals such as Fe (57, 58), Mn (59, 60), and Ru (61–63). Finally, reaction of the $[Ru^{(IV)}]$-OH species with $HCOOCH_3$ would yield Fig. 4, **7**. The optimized structures of Fig. 4, **6** and **7** have real frequencies in density functional theory calculations [DFT; calculations performed using Gaussian 09 (64); spin unrestricted orbitals and exchange correlation was treated at the B3LYP (Becke, three-parameter, Lee–Yang–Par) hybrid functional level (65, 66); DGDZVP (density Gauss double-zeta with polarization functions) (67) full electron basis set was used with the density Gaussian fitting basis set DGA1 (67, 68)], indicating that the proposed structures for these intermediates are feasible (see *SI Appendix* for DFT parameters). Optimized structures for Fig. 4, **6** and **7** have η^6-*p*-cymene configurations (*SI Appendix*, Fig. S12) and the calculated distances for the [Ru]—O and [Ru]—N bonds (*SI Appendix*, Table S4) agree with the proposed structures shown in Fig. 4. In addition, tandem MS experiments show that the species at nominal m/z 444 and m/z 460 both dissociate to yield an isotope distribution at nominal m/z 384, corresponding to the protonated form of Fig. 4, **4**, which is the base structure for Fig. 4, **6** and **7** (*SI Appendix*, Fig. S13). The dissociation profile for Fig. 4, **6** and **7** as a function of normalized collision energy (*SI Appendix*, Fig. S14) indicates that Fig. 4, **6** is less stable compared to Fig. 4, **7**, which is expected because the organic substituent is more weakly bound in Fig. 4, **6**. All these results provide support for the identification of intermediates that are formed from reaction intermediates that react with $HCOOCH_3$ (i.e., Fig. 4, **6** and **7**).

The results described in this study show that Ru-methyl formate intermediates are formed when methanol reacts with (β-amino alcohol)(arene)RuCl complexes. The short reaction time in microdroplets from DESI allowed these transient species to be intercepted on the millisecond time scale (36) and the use of a high-resolution mass spectrometer permits unambiguous identification. These discoveries provide information on unique transient intermediates in transfer hydrogenation as well as possible pathways that inhibit the catalytic cycle in solution, thereby facilitating the design and optimization of more efficient CTH catalysts. This report also shows that DESI is a simple and powerful way to follow complex reactions on short time scales that recommends itself for many other applications.

Methods

Desorption Electrospray Ionization Mass Spectrometry. The amino alcohol (1*R*, 2*S*)-*cis*-1-amin-2-indanol (Fig. 1, **2**; 10^{-4} M in CH_3OH) was infused through a fused silica (FS) capillary tubing (100 μm i.d., 360 μm o.d.) of a custom-built DESI source at a rate of 20 μL/min. Unless specified otherwise all chemicals were purchased from Sigma-Aldrich and used without further processing. For experiments with base a solution containing 10^{-4} M KOH; 10^{-4} M Fig. 1, **2**; and CH_3OH was used as the DESI spray. The FS passes through the 180° openings of a 1/16 inch stainless steel (SS) tee. At the opening closest to the solvent reservoir, the FS is held in place using a vespel ferrule (400 μm i.d.). A stainless steel tubing (approximately 500 μm i.d., 1/16 inch o.d., 5 cm length) is attached to the other 180° opening of the SS tee making a sheath that surrounds the FS. The FS protrudes from the SS tube by approximately 1 mm–2 mm. The N_2 source is attached to the 90° opening of the SS tee. The N_2 flow rate is approximately 1 L/min. The DESI source is positioned at a 45° angle to the surface, 2 mm above the surface, and at a distance of 5 mm from the inlet of an Orbitrap mass spectrometer (*SI Appendix*, Fig. S1). The $RuCl_2$ *p*-cymene dimer (Fig. 1, **1**; 10^{-2} M in CH_2Cl_2) was deposited (5 μL) on paper that is affixed to a glass slide. When the primary droplets containing Fig. 1, **2** (5 kV or 0 kV spray voltage) impact Fig. 1, **1** on the surface the reaction is initiated and then proceeds in secondary microdroplets (*SI Appendix*, Fig. S1). The Orbitrap ion transfer capillary was held at 200 °C, resolution was set to 100,000 at m/z 400, and data were collected in full scan mode (m/z 150–m/z 1,500). MS/MS experiments were carried out using an LCQ Deca XP quadrupole ion trap mass spectrometer (isolation width = 5 m/z units; activation time = 100 ms; q = 0.25; Thermo Fisher Scientific). MS/MS spectra were recorded for m/z 444 and m/z 460 as a function of normalized collision energy, which was varied from 0%–50%.

Nuclear Magnetic Resonance and Gas Chromatography-Mass Spectrometry Analyses of the Bulk Reaction Mixture. Anhydrous CH_3OH was purchased from Sigma-Aldrich, dried over CaH_2, vacuum transferred, and stored under argon and activated 3 Å molecular sieves. CD_3CN was purchased from Cambridge Isotope Laboratories and was dried over calcium hydride (CaH_2), transferred under reduced pressure, and stored in an inert atmosphere over activated 3 Å molecular sieves. Fig. 1, **1** and **2** were purchased from Strem Chemicals, Inc., stored in an inert atmosphere glove box, and then used without further processing. KOH was dried in vacuum (24 mtorr) at 61 °C for 1 week prior to use. The Ru-Cl Fig. 1, **3** (10 mg, 0.0239 mmol) and KOH (6.5 mg, 0.1195 mmol) were weighed into a sealable NMR tube. CD_3CN (0.5 mL) and CH_3OH (6.8 μL, 0.167 mmol) were added via syringe. The reaction was monitored via ^1H NMR (field strength = 600 MHz; temperature = 25 °C). A portion of the NMR sample was diluted with diethyl ether, filtered, and analyzed by GC-MS (single quadrupole mass analyzer; electron impact ionization; 70 eV electron energy; model 7890/5795 from Agilent Technologies). The GC column (0.25 mm i.d.; model HP-5MSi from Agilent Technologies) was 30 m long and contained (5% phenyl)-methylpolysiloxane (25 μm film thickness). A standard sample of $HCOOCH_3$ in diethyl ether was analyzed by GC-MS using the parameters described above.

ACKNOWLEDGMENTS. We are indebted to Antonio De Crisci (Stanford University) for his help with determining reasonable structures for the intermediates and potential reaction mechanisms. We also thank Pavel Aronov and Allis Chien (Stanford University Mass Spectrometry) for providing instrumentation and their expertise in the field of mass spectrometry. R.H.P. thanks the Center for Molecular Analysis and Design at Stanford University (1123893-1-AABGE) and K.C. the Swiss National Science Foundation (PBEZP2-133126) for postdoctoral fellowships. K.R.B. thanks the Center for Molecular Analysis and Design at Stanford University (1134697-1-EANUU) for funding. T.J.C. acknowledges the Department of Defense for a National Defense and Science Engineering Graduate Research Fellowship. Financial support from the Air Force Office of Scientific Research (FA 9550-10-1-0235) is gratefully acknowledged.

1. Brieger G, Nestrick TJ (1974) Catalytic transfer hydrogenation. *Chem Rev* 74:567–580.
2. Gladiali S, Alberico E (2006) Asymmetric transfer hydrogenation: Chiral ligands and applications. *Chem Soc Rev* 35:226–236.
3. Palmer MJ, Wills M (1999) Asymmetric transfer hydrogenation of C=O and C=N bonds. *Tetrahedron Asymmetry* 10:2045–2061.
4. Wang C, Wu XF, Xiao JL (2008) Broader, greener, and more efficient: Recent advances in asymmetric transfer hydrogenation. *Chem-Asian J* 3:1750–1770.
5. Clapham SE, Hadzovic A, Morris RH (2004) Mechanisms of the H_2-hydrogenation and transfer hydrogenation of polar bonds catalyzed by ruthenium hydride complexes. *Coord Chem Rev* 248:2201–2237.
6. Ashby EC (1988) Single-electron transfer, a major reaction pathway in organic chemistry. An answer to recent criticisms. *Acc Chem Res* 21:414–421.
7. Shiner VJ, Jr, Whittaker D (1969) Kinetics of the Meerwein–Ponndorf–Verley reaction. *J Am Chem Soc* 91:394–398.
8. Ruiz JR, Jimenez-Sanchidrian C (2007) Heterogeneous catalysis in the Meerwein–Ponndorf–Verley reduction of carbonyl compounds. *Curr Org Chem* 11:1113–1125.
9. Klomp D, Hanefeld U, Peters JA (2007) *Transfer Hydrogenation Including the Meerwein–Ponndorf–Verley Reduction* (Wiley-VCH GmbH & Co. KGaA, Weinheim, Berlin, Germany), pp 585–630.
10. Fuchter MJ (2007) *Oppenauer Oxidation* (John Wiley & Sons, Inc, Hoboken, NJ), pp 265–273.
11. Palmer M, Walsgrove T, Wills M (1997) (1***R***,2***S***)-(+)-*cis*-1-amino-2-indanol: An effective ligand for asymmetric catalysis of transfer hydrogenations of ketones. *J Org Chem* 62:5226–5228.
12. Haack KJ, Hashiguchi S, Fujii A, Ikariya T, Noyori R (1997) The catalyst precursor, catalyst, and intermediate in the Ru-II-promoted asymmetric hydrogen transfer between alcohols and ketones. *Angew Chem Int Ed* 36:285–288.
13. Smith TA, Aplin RP, Maitlis PM (1985) The ruthenium-catalyzed conversion of methanol into methyl formate. *J Organomet Chem* 291:C13–C14.
14. Yang LC, Ishida T, Yamakawa T, Shinoda S (1996) Mechanistic study on dehydrogenation of methanol with $RuCl_2(PR_3)_3$ -type catalyst in homogeneous solutions. *J Mol Catal A-Chem* 108:87–93.
15. Kenny JA, Versluis K, Heck AJR, Walsgrove T, Wills M (2000) The detection of intermediates in the ruthenium (II) catalysed asymmetric hydrogenation of ketones using electrospray ionisation mass spectrometry. *Chem Commun* 99–100.
16. Noyori R, Hashiguchi S (1997) Asymmetric transfer hydrogenation catalyzed by chiral ruthenium complexes. *Acc Chem Res* 30:97–102.
17. Noyori R, Ohkuma T (2001) Asymmetric catalysis by architectural and functional molecular engineering: Practical chemo- and stereoselective hydrogenation of ketones. *Angew Chem Int Ed* 40:40–73.
18. Noyori R, Takaya H (1990) BINAP—An efficient chiral element for asymmetric catalysis. *Acc Chem Res* 23:345–350.
19. Noyori R, Yamakawa M, Hashiguchi S (2001) Metal–ligand bifunctional catalysis: A nonclassical mechanism for asymmetric hydrogen transfer between alcohols and carbonyl compounds. *J Org Chem* 66:7931–7944.
20. Takehara J, et al. (1996) Amino alcohol effects on the ruthenium (II)-catalysed asymmetric transfer hydrogenation of ketones in propan-2-ol. *Chem Commun* 233–234.
21. Adlhart C, Chen P (2000) Fishing for catalysts: Mechanism-based probes for active species in solution. *Helv Chim Acta* 83:2192–2196.
22. Chen P (2003) Electrospray ionization tandem mass spectrometry in high-throughput screening of homogenous catalysts. *Angew Chem Int Ed* 42:2832–2847.
23. Eberlin MN (2007) Electrospray ionization mass spectrometry: A major tool to investigate reaction mechanisms in both solution and the gas phase. *Eur J Mass Spectrom* 13:19–28.
24. Cooks RG, Ouyang Z, Takats Z, Wiseman JM (2006) Ambient mass spectrometry. *Science* 311:1566–1570.
25. Ifa DR, Wu CP, Ouyang Z, Cooks RG (2010) Desorption electrospray ionization and other ambient ionization methods: Current progress and preview. *Analyst* 135:669–681.
26. Venter A, Nefliu M, Cooks RG (2008) Ambient desorption ionization mass spectrometry. *Trac Trends Anal Chem* 27:284–290.
27. Girod M, Moyano E, Campbell DI, Cooks RG (2011) Accelerated bimolecular reactions in microdroplets studied by desorption electrospray ionization mass spectrometry. *Chem Sci* 2:501–510.
28. Takats Z, Wiseman JM, Cooks RG (2005) Ambient mass spectrometry using desorption electrospray ionization (DESI): Instrumentation, mechanisms and applications in forensics, chemistry, and biology. *J Mass Spectrom* 40:1261–1275.
29. Takats ZW, Wiseman JM, Gologan B, Cooks RG (2004) Mass spectrometry sampling under ambient conditions with desorption electrospray ionization. *Science* 306:471–473.
30. Coelho F, Eberlin MN (2011) The bridge connecting gas-phase and solution chemistries. *Angew Chem Int Ed* 50:5261–5263.
31. Marquez CA, Wang HY, Fabbretti F, Metzger JO (2008) Electron-transfer-catalyzed dimerization of trans-anethole: Detection of the distonic tetramethylene radical cation intermediate by extractive electrospray ionization mass spectrometry. *J Am Chem Soc* 130:17208–17209.
32. McCullough BJ, Bristow T, O'Connor G, Hopley C (2011) On-line reaction monitoring by extractive electrospray ionisation. *Rapid Commun Mass Spectrom* 25:1445–1451.
33. Miao ZX, Chen H, Liu PY, Liu Y (2011) Development of submillisecond time-resolved mass spectrometry using desorption electrospray ionization. *Anal Chem* 83:3994–3997.
34. Miao ZX, Wu SY, Chen H (2010) The study of protein conformation in solution via direct sampling by desorption electrospray ionization mass spectrometry. *J Am Soc Mass Spectrom* 21:1730–1736.
35. Xu GM, Chen B, Guo B, He DX, Yao SZ (2011) Detection of intermediates for the Eschweiler–Clarke reaction by liquid-phase reactive desorption electrospray ionization mass spectrometry. *Analyst* 136:2385–2390.
36. Perry RH, Splendore M, Chien A, Davis N, Zare RN (2011) Detecting reaction intermediates in liquids on the millisecond time scale using desorption electrospray ionization. *Angew Chem Int Ed* 50:250–254.
37. Hu QZ, et al. (2005) The Orbitrap: A new mass spectrometer. *J Mass Spectrom* 40:430–443.
38. Makarov A, et al. (2006) Performance evaluation of a hybrid linear ion trap/orbitrap mass spectrometer. *Anal Chem* 78:2113–2120.
39. Perry RH, Cooks RG, Noll RJ (2008) Orbitrap mass spectrometry: Instrumentation, ion motion, and applications. *Mass Spectrom Rev* 27:661–699.
40. Pearson DM, Waymouth RM (2009) Mechanistic studies of the oxidative dehydrogenation of methanol using a cationic palladium complex. *Organometallics* 28:3896–3900.
41. Starchevsky MK, Hladiy SL, Pazdersky YA, Vargaftik MN, Moiseev II (1999) Giant Pd-561 clusters: Inset to new catalytic properties. *J Mol Catal A-Chem* 146:229–236.
42. Lastovyak YV, et al. (1994) Methanol oxidation catalyzed with a giant palladium cluster. *Kinet Catal* 35:512–515.
43. Nishimura T, Kakiuchi N, Onoue T, Ohe K, Uemura S (2000) Palladium (II)-catalyzed oxidation of terminal alkenes to methyl ketones using molecular oxygen. *J Chem Soc-Perkin Trans* 1:1915–1918.
44. Venter A, Sojka PE, Cooks RG (2006) Droplet dynamics and ionization mechanisms in desorption electrospray ionization mass spectrometry. *Anal Chem* 78:8549–8555.
45. Kumar P, et al. (2010) Synthesis, characterization and reactivity of arene ruthenium compounds based on 2,2′-dipyridylamine and di-2-pyridylbenzylamine and their applications in catalytic hydrogen transfer of ketones. *J Organomet Chem* 695:2205–2212.
46. Abdur-Rashid K, et al. (2002) Mechanism of the hydrogenation of ketones catalyzed by trans-dihydrido(diamine)ruthenium(II) complexes. *J Am Chem Soc* 124:15104–15118.
47. Wu XF, Xiao JL (2007) Aqueous-phase asymmetric transfer hydrogenation of ketones—a greener approach to chiral alcohols. *Chem Commun* 2449–2466.
48. Cant NW, Tonner SP, Trimm DL, Wainwright MS (1985) Isotopic labeling studies of the mechanism of dehydrogenation of methanol to methyl formate over copper-based catalysts. *J Catal* 91:197–207.
49. Iwasa N, Yamamoto O, Akazawa T, Ohyama S, Takezawa N (1991) Dehydrogenation of methanol to methyl formate over palladium zinc-oxide catalysts. *J Chem Soc-Chem Commun* 1322–1323.
50. Liu ZT, Lu DS, Guo ZY (1994) Polyacrylonitrile coated silica as a support for copper catalyst in methanol dehydrogenation to methyl formate. *Appl Catal A-Gen* 118:163–171.
51. Miyazaki E, Yasumori I (1967) Kinetics of catalytic decomposition of methanol formaldehyde and methyl formate over a copper-wire surface. *Bull Chem Soc Jpn* 40:2012–2017.
52. Pocker Y, Davis BC (1974) Mechanism of methanol oxidation by lead-tetraacetate—novel intermediacy of formaldehyde hemiacetal. *J Chem Soc-Chem Commun* 803–804.
53. Heiden ZM, Rauchfuss TB (2007) Homogeneous catalytic reduction of dioxygen using transfer hydrogenation catalysts. *J Am Chem Soc* 129:14303–14310.
54. Arita S, Koike T, Kayaki Y, Ikariya T (2008) Aerobic oxidation of alcohols with bifunctional transition-metal catalysts bearing C-N chelate ligands. *Chem Asian J* 3:1479–1485.
55. Chowdhury S, Himo F, Russo N, Sicilia E (2010) Mechanistic investigation of the hydrogenation of O_2 by a transfer hydrogenation catalyst. *J Am Chem Soc* 132:4178–4190.
56. Jiang B, Feng Y, Ison EA (2008) Mechanistic investigations of the iridium(III)-catalyzed aerobic oxidation of primary and secondary alcohols. *J Am Chem Soc* 130:14462–14464.
57. Nam W (2007) High-valent iron (IV)-oxo complexes of heme and non-heme ligands in oxygenation reactions. *Acc Chem Res* 40:522–531.
58. Groves JT, Watanabe Y (1988) Reactive iron porphyrin derivatives related to the catalytic cycles of cytochrome-P-450 and peroxidase—studies of the mechanism of oxygen activation. *J Am Chem Soc* 110:8443–8452.
59. Yachandra VK, Sauer K, Klein MP (1996) Manganese cluster in photosynthesis: Where plants oxidize water to dioxygen. *Chem Rev* 96:2927–2950.
60. Fukuzumi S, et al. (2009) Mechanistic insights into hydride-transfer and electron-transfer reactions by a manganese (IV)-oxo porphyrin complex. *J Am Chem Soc* 131:17127–17134.
61. Huynh MHV, Meyer TJ (2007) Proton-coupled electron transfer. *Chem Rev* 107: 5004–5064.
62. Kojima T, et al. (2010) A low-spin ruthenium (IV)-oxo complex: Does the spin state have an impact on the reactivity? *Angew Chem Int Ed* 49:8449–8453.
63. Singh P, Singh AK (2010) Transfer hydrogenation of ketones and catalytic oxidation of alcohols with half-sandwich complexes of ruthenium (II) designed using benzene and tridentate (S, N, E) type ligands (E = S, Se, Te). *Organometallics* 29:6433–6442.
64. Frisch MJ, et al. (2009) Gaussian 09, Revision A01. Gaussian, Inc., Wallingford CT.
65. Becke AD (1988) Density-functional exchange-energy approximation with correct asymptotic-behavior. *Phys Rev A* 38:3098–3100.
66. Lee CT, Yang WT, Parr RG (1988) Development of the Colle–Salvetti correlation-energy formula into a functional of the electron-density. *Phys Rev B* 37:785–789.
67. Godbout N, Salahub DR, Andzelm J, Wimmer E (1992) Optimization of gaussian-type basis sets for local spin-density functional calculations. 1. Boron through neon, optimization technique and validation. *Can J Chem-Rev Can Chim* 70:560–571.
68. Sosa C, et al. (1992) A local density functional-study of the structure and vibrational frequencies of molecular transition-metal compounds. *J Phys Chem* 96:6630–6636.